
SUPPLEMENTARY INFORMATION

Engineering thermal rectification in MoS₂ nanoribbons: a non-equilibrium molecular dynamics study

Leonardo Medrano Sandonas,^{a,b,c} Rafael Gutierrez,^{*a,c} Arezoo Dianat,^{a,c} and Giovanni Cuniberti^{a,c,d}

^a Institute for Materials Science and Max Bergmann Center of Biomaterials, TU Dresden, 01062 Dresden, Germany. Fax: +49 (0)351 4633 1422; Tel: +49 (0)351 4633 1419; E-mail:

rafael.gutierrez@nano.tu-dresden.de

^b Max Planck Institute for the Physics of Complex Systems, 01187 Dresden, Germany

^c Dresden Center for Computational Materials Science (DCCMS), TU Dresden, 01062 Dresden, Germany

^d Center for Advancing Electronics Dresden, TU Dresden, 01062 Dresden, Germany

1 Molecular dynamics (MD) simulation

1.1 Benchmarking of the MD parameters

A first step before addressing the issue of thermal transport, was to implement a reliable force field for MoS₂ in LAMMPS code. Then, we found accurate simulation parameters to perform the non-equilibrium molecular dynamics simulations. To do this task, we did a systematic study of the parameters related to the heat baths. We have selected the Nosé-Hoover (NH) thermostat for the heat baths in order to have a good performance reproducing the canonical ensemble and avoid artifacts which have been reported by using, e.g., Berendsen thermostat.¹ In the scheme of the NH thermostat, the equation of motion for a particle i in the heat bath is:

$$\frac{d\mathbf{q}_i}{dt} = \frac{\partial H}{\partial \mathbf{p}_i}, \quad \frac{d\mathbf{p}_i}{dt} = -\frac{\partial H}{\partial \mathbf{q}_i} - \xi \mathbf{p}_i, \quad (1)$$

where H is the Hamiltonian of the system, \mathbf{p}_i and \mathbf{q}_i are the momentum and coordinate of particle i , respectively, and ξ is an auxiliary variable modeling the microscopic action of the heat bath. The dynamics of ξ is governed by the following equation:

$$\frac{d\xi}{dt} = \frac{1}{\tau^2} \left[\frac{T(t)}{T_0} - 1 \right], \quad T(t) = \frac{2}{3Nk_B} \sum_i \frac{\mathbf{p}_i \cdot \mathbf{p}_i}{2m_i}, \quad (2)$$

where k_B is the Boltzmann constant, m_i is the mass of the particle i , T_0 and τ are the aimed temperature and the relaxation time of the heat bath, respectively, and N is the total number of particles that is in contact with heat bath.

After selecting the thermostat, the first fixed parameter was the length of the heat bath, L_{HB} . In our calculations, we have considered as mean temperature 300 K and the temperature bias $\Delta T = 60$ K, i.e., $T_L = 330$ K and $T_R = 270$ K for the forward direction and $T_L = 270$ K and $T_R = 330$ K for the backward direction of the heat flux. In Fig. 1 we show the effect of the number of heat bath layers on the temperature profile of a symmetric MoS₂ nanoribbon ($W_{LR} = 1.0$). The bath relaxation time $\tau = 0.1$ was used for this study. A linear temperature gradient is observed in the inner part of the device region. The main difference in temperature profile between different heat bath conditions is the temperature jump between the heat bath and interior layers. With the number of heat bath layers increasing, the temperature jump is reduced as shown in Fig. 1, this effect leading to an increase in the heat flux (see Table 1). Further increase in the

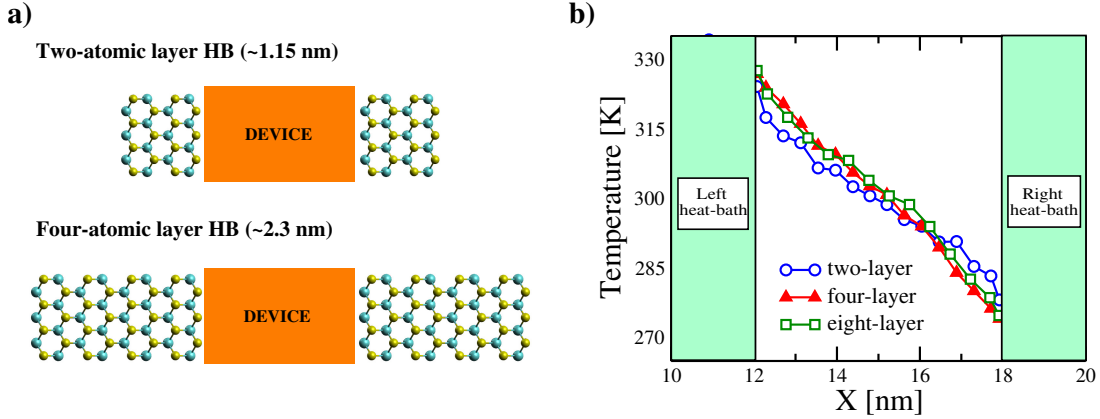


Figure 1 a) Schematic of MoS₂ nanoribbons with different heat bath lengths. b) Variation of the temperature profile with the heat bath length for symmetric MoS₂ nanoribbons in the forward direction of the heat flux.

Table 1 Values of the heat flux and thermal rectification for different length of the heat bath

		Length of the heat bath, L_{HB}		
		2-layer (~1.15 nm)	4-layer (~2.3 nm)	8-layer (~4.6 nm)
Heat flux [$\times 10^{-7}$ W]	forward	0.6856	0.8866	1.0367
	backward	0.6976	0.8937	1.0397
Thermal rectification, η		1.72 ± 0.1	0.79 ± 0.2	0.29 ± 0.1

number of heat bath layers cannot eventually remove the temperature jump. The small remaining temperature jump is due to the thermal boundary resistance (TBR) between heat bath and the device region, which is the result of the mismatch in their corresponding phonon density of states². A similar effect has been reported for carbon nanotubes,^{2,3} and silicon nanowires.¹ In addition, we have calculated the sensitivity of the thermal rectification as a function of the heat bath length. It turned out that for small lengths the thermal rectification for *symmetric* MoS₂ nanoribbons was different from zero but, after increasing L_{HB} , this value converged to zero as expected for symmetric geometries. The threshold value for this behavior was $L_{HB} \sim 2.3$ nm. All the following calculations were thus carried out with this bath length.

Regarding the relaxation time, τ , it is well-known that the temperature profile has a strong dependence on the magnitude of this parameter. For instance, τ should not be too small compared to the time step because it can cause large oscillations in temperature. Such oscillations can lead to the accumulation of numerical errors, causing the system to deviate from the canonical distribution. Such numerical error accumulation can also happen if the relaxation time is very large because the total simulation time becomes very long. Here, we set $L_{HB} = 2.3$ nm (4 atomic layers) to perform this study. As it is shown in Fig. 2, we have found that the temperature profile for MoS₂ nanoribbon with $W_{LR} = 1.0$ is strongly depended on this parameter. In fact, despite the heat bath reaching the target temperature and the temperature profile being well defined for $\tau = 0.001$, the heat flux for the hot and cold heat bath are rather different at steady state, which is not the correct thermodynamic behavior. In the case of large relaxation time, we found that the MoS₂ nanoribbons display a wrong temperature profile for both directions of the heat flux. The heat baths do not reach the target temperature. Similar behaviors have been reported for other nanomaterials.^{1,2} Thus, our results indicate that the steady state temperature or heat current distribution do not depend on any particular value of the relaxation time in the range from 0.01 ps to 1 ps. Hence, in the present work, we chose $\tau = 0.1$ ps for the MD simulations, which is large

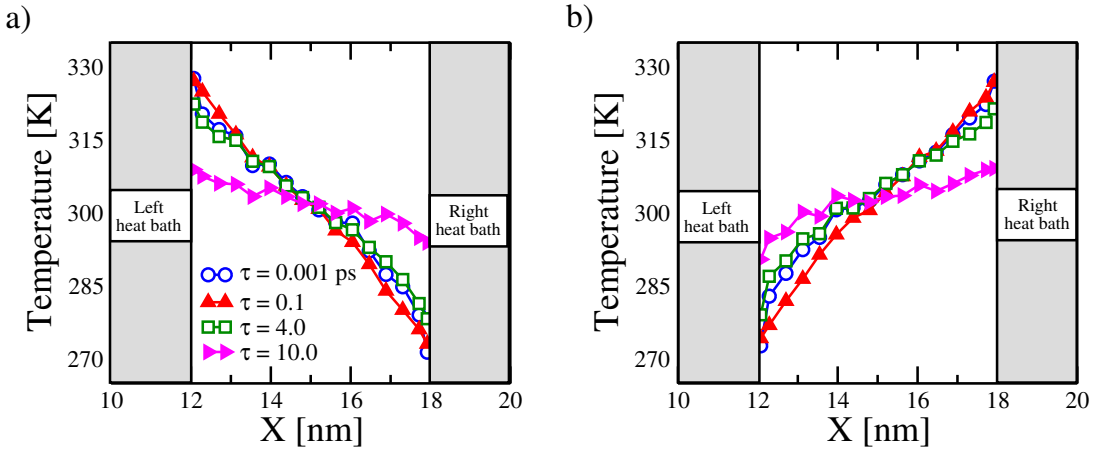


Figure 2 Relaxation time dependence of the temperature profile for symmetric MoS₂ nanoribbons in the a) forward and b) backward direction of the heat flux.

Table 2 Values of the heat flux and thermal rectification for different relaxation time of the heat bath

		Relaxation time of the heat bath, τ		
		0.1	4.0	10.0
Heat flux [$\times 10^{-7}$ W]	forward	0.8866	0.5132	0.3041
	backward	0.8937	0.5159	0.3063
Thermal rectification		0.79 ± 0.2	0.52 ± 0.1	0.72 ± 0.1

enough to avoid high frequency temperature oscillations, and leads to a stabilization time (the time needed to reach the steady state in the simulation) of about 1.0 ns, which is short enough to avoid large numerical error accumulation. It is worth mentioning that despite the relaxation time dependence of the temperature profile in MoS₂ nanoribbons, the magnitude of the thermal rectification is only slightly affected because of the symmetry of the temperature profile when the temperature bias is reversed (see Table 2).

1.2 Influence on the Mo-S bond length

In Fig. 3, we show the statistical distribution for the fluctuations of the Mo-S bond length b during the non-equilibrium molecular dynamics simulation in forward and backward directions of the heat flux. The calculations have been done after the system reached the steady state, i.e., during the last 10 ns. The obtained equilibrium length for Mo-S bond is $b_0 = 2.8 \text{ \AA}$ (for the relaxed structure). The figure shows the maximum variation for the bond length $\Delta b = b - b_0$, independently if the atoms are located on the center or edge, is 0.1 \AA . These results are the average of 30 different bond length which have been randomly taking for the corresponding sectors of the device. Therefore, the Mo-S bond length during the NEMD simulation is only affected up to 3.5 % of its equilibrium value.

2 Real-space vibrational mode analysis

As it was discussed in the main text, we have used a real-space analysis for rationalizing the behavior of the vibrational modes in asymmetric MoS₂ nanoribbons and trying to establish a connection to the rectification behavior. To find the frequencies ω_λ and their corresponding vector components $\epsilon_{i\alpha,\lambda}$ of the vibrational modes, we first solved the lattice

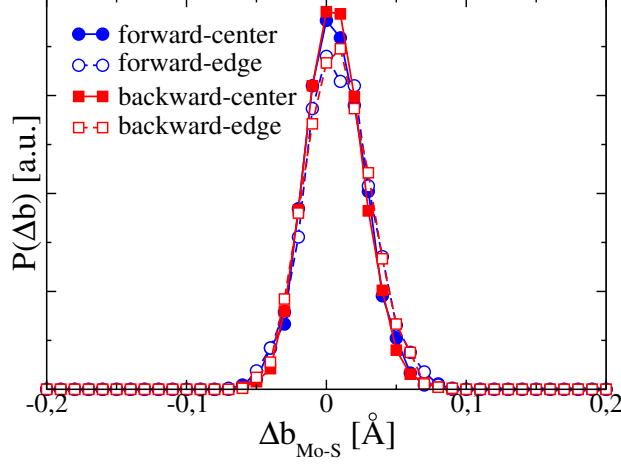


Figure 3 Distribution of the variations of Mo-S bond length during the non-equilibrium molecular dynamics simulation in forward and backward direction of the heat flux. We show the results for the atoms located on the center and edge parts.

dynamical equations:⁴

$$\omega_\lambda^2 \varepsilon_{i\alpha,\lambda} = \sum_{j\beta} \Phi_{i\alpha,j\beta} \varepsilon_{j\beta,\lambda}, \quad (3)$$

where Φ is the mass-weighted matrix and its elements are given as

$$\Phi_{i\alpha,j\beta} = \frac{1}{\sqrt{m_i m_j}} \frac{\partial^2 V}{\partial u_{i\alpha} \partial u_{j\beta}}, \quad (4)$$

Here $u_{i\alpha}$ is the displacement of ion i in the α Cartesian direction, m_i is the mass of ion i , and V is the total potential energy employed for the molecular dynamics simulation. The Hessian matrix is calculated numerically using a finite-difference approach involving very small atomic displacements. The vibrational modes of the MoS₂ nanoribbons with N atoms were calculated by diagonalizing the $3N \times 3N$ matrix given by eq. 4.

Fig. 4 complements the results presented in a similar figure in the main text (Fig. 4). Here, we show the spatial distribution of the vibrational modes, as given by the function $\phi_{i\alpha,\Lambda}$, for the other two intervals of the participation ratio defined in the main text (see also the middle panel of Fig. 4): I) $p > 0.4$ and II) $0.1 < p < 0.4$, for the forward and backward directions of the heat flux. For case I (Fig. 4a,c), which corresponds to a subset of rather delocalized modes, it turns out that a major contribution to these modes is coming from atoms along the edges of the nanoribbon (both Mo and S atoms), while the bulk contributions are much weaker (values of $\phi_{i\alpha,\Lambda} \leq 2$). In case II (see Fig. 4b,d) the behavior is more complex: sulfur atoms in the center and edges of the ribbon give the strongest contribution, while molybdenum atoms are basically "silent", a fact related to the previously found result that in the spectral range 230-370 cm⁻¹ the Mo atoms do not appreciably contribute to the vibrational density of states. By comparing Fig. 4a,b with Fig. 4c,d, the spatial distribution of the vibrational modes in backward direction is similar to the obtained in the forward direction. A rather similar behavior was found for trapezoidal MoS₂ nanoribbons of length $L = 5.9$ nm and $W_{LR} = 3.0$ as shown in Fig. 5. Notice that the largest changes in the spatial distribution of modes upon inversion of the heat flow direction takes place for the spectral range III with the smallest participation ratio. This behavior shows the same qualitative tendency as for the previously discussed T-shape nanoribbon. Thus, our results suggest that for the considered asymmetric nanoribbons, modes located within the spectral range from 350 cm⁻¹ to 600 cm⁻¹ are providing the main contribution to the thermal rectification, since they are the most affected by the inversion of the heat flow. On the other hand, the precise asymmetric shape of the ribbon seems to mainly determine the size of

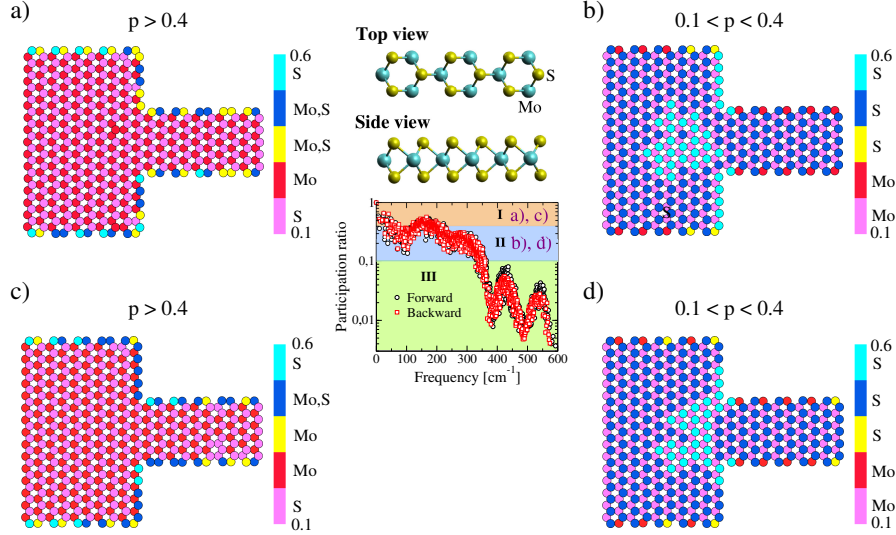


Figure 4 Spatial distributions, ϕ , of vibrational modes for T-shaped MoS_2 nanoribbons of $L = 5.9$ nm and $W_{\text{LR}} = 3.0$ (XY plane). We have considered two restrictions based on the magnitude of the participation ratio, p : I) $p > 0.4$ and II) $0.1 < p < 0.4$ for the system obtained after NEMD simulation in the forward (a) and b)) and backward (c) and d)) direction. We have considered $\alpha = 0.1$ for this calculation. The color scale has the same meaning for all the cases, i.e., cyan balls mean highest contribution while pink balls lowest contribution for the vibrational modes. In these pictures, we only show the contributions arising from the top S-layer as well as the Mo-layer.

the thermal rectification.

Furthermore, we have calculated some extra quantities to explore additional features of the vibrational modes in the device region. We have thus studied the polarization vector $e_{i\alpha,\lambda}$ of an atom i , for a given mode λ , which is defined as

$$e_{i\alpha,\lambda} = \frac{\epsilon_{i\alpha,\lambda}}{\sum_{\alpha} \epsilon_{i\alpha,\lambda}^* \epsilon_{i\alpha,\lambda}}. \quad (5)$$

In a crystal without defects, the normal modes are all phonon modes and possess well-defined polarization vectors⁵. For example, for an LA mode, if the polarization vector is parallel to \mathbf{k} (say, the Z direction), then each ion has a unit polarization vector component of ± 1 in the Z direction and 0 in the X and Y directions. In Fig. 6, we show the projections of the polarization vectors onto the Y - X and the Z - Y planes for the T-shaped MoS_2 nanoribbon with $W_{\text{LR}} = 3.0$ after NEMD simulations with heat flowing in the forward direction. We have selected only three representative frequencies for this analysis: 50 cm^{-1} (Fig. 6a,d), 350 cm^{-1} (Fig. 6b,e), and 560 cm^{-1} (Fig. 6c,f). The results show that frequencies $< 90 \text{ cm}^{-1}$ behave like a *propagon* mode, while frequencies between 90 cm^{-1} and 550 cm^{-1} are *diffuson* modes with frequency dependence of their participation ratio. Highest frequencies, $> 550 \text{ cm}^{-1}$, tend to have a unit polarization vector component in the Z direction and are expected to be *locon* modes as discussed in the context of amorphous systems⁴. Hence, we have that the atoms are essentially vibrating in the plane during the NEMD simulation but this phenomena depends on the frequency of the vibrational mode. We have also found similar behavior for the other geometries studied in the present work.

Another relevant quantity is the phase quotient Φ_{λ} of a mode λ , which is given by

$$\Phi_{\lambda} = \frac{\sum_{\langle i,j \rangle} (\sum_{\alpha} \epsilon_{i\alpha,\lambda} \epsilon_{j\alpha,\lambda})}{\sum_{\langle i,j \rangle} |\sum_{\alpha} \epsilon_{i\alpha,\lambda} \epsilon_{j\alpha,\lambda}|}, \quad (6)$$

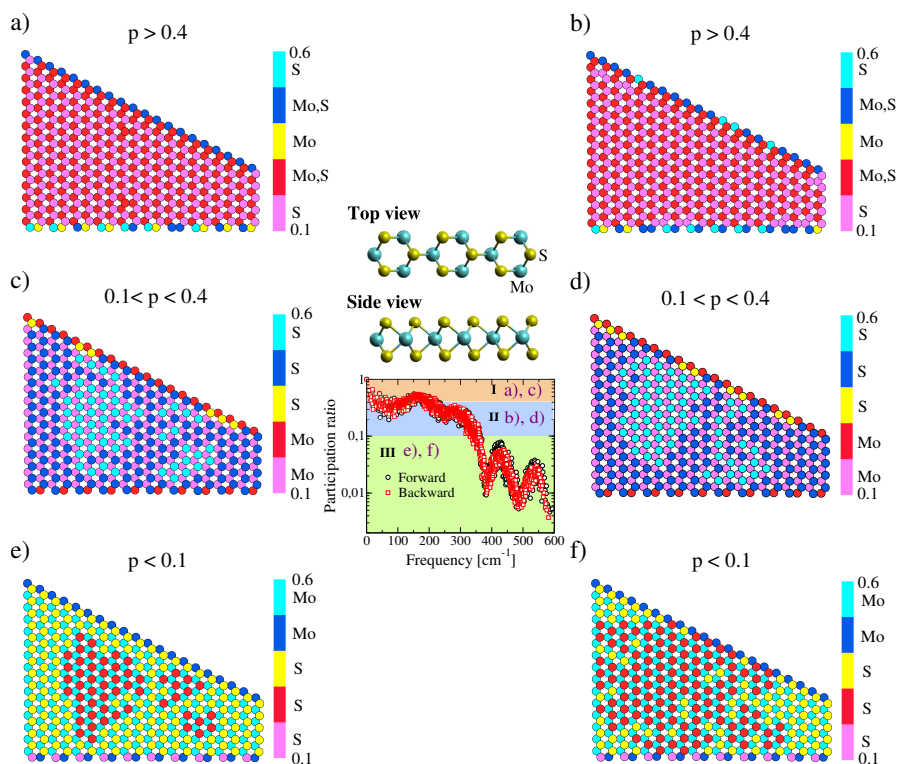


Figure 5 Spatial distributions, ϕ , of vibrational modes for trapezoidal MoS_2 nanoribbons of $L = 5.9$ nm and $W_{\text{LR}} = 3.0$ (XY plane). We have considered three restrictions based on the magnitude of the participation ratio, p : I) $p > 0.4$, II) $0.1 < p < 0.4$, and III) $p < 0.1$ for the system obtained after NEMD simulation in the forward (a), c), and e)) and backward (b), d), and f)) direction. We have considered $\alpha = 0.1$ for this calculation. The color scale has the same meaning for all the cases, i.e., cyan balls mean highest contribution while pink balls lowest contribution for the vibrational modes. In these pictures, we only show the contributions arising from the top S-layer as well as the Mo-layer.

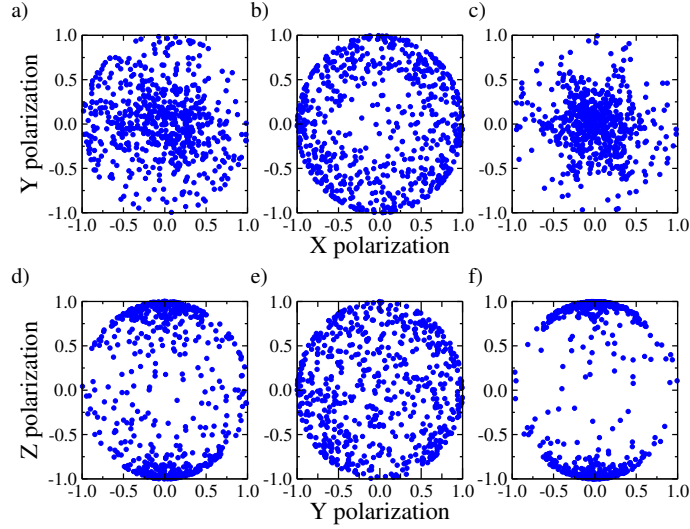


Figure 6 Projections of the polarization vectors onto Y-X and Z-Y planes for the T-shaped MoS₂ nanoribbon with $W_{LR} = 3.0$ after NEMD simulation in the forward direction ($T_0 = 300$ K and $\alpha = 0.1$) in the frequencies: 50 cm^{-1} (a,d), 350 cm^{-1} (b,e), and 560 cm^{-1} (c,f).

where i and j are nearest neighbors. As is shown in Figure 7, for low frequencies values of Φ_λ near 1.0 indicate that nearest-neighbors atoms vibrate mostly in-phase like an acoustic mode, while, for high frequencies, values near -1 indicate that they vibrate out-of-phase in a manner characteristic of an optical mode. The frequency dependence of the phase quotient for the T-shaped MoS₂ nanoribbon with $W_{LR} = 3.0$, after a NEMD simulation in forward or backward direction, forms a band of monotonically decreasing values. However, there is an increase of phase quotient in the range $200\text{-}230 \text{ cm}^{-1}$. As was reported in Ref. 4, this increase coincides with the end of the transverse acoustic TA branch in MoS₂ bulk which is 210 cm^{-1} . Moreover, in this range the vibrational density of states has a local minimum. As the TA branch ends, the modes begin to acquire features akin to LA, leading to an increase in the phase quotient. These properties have been properly invoked for diffusion modes in amorphous silicon, but apparently similar physics is taking place in asymmetric MoS₂ nanoribbons because of the finite size effects and the non-equilibrium conditions.

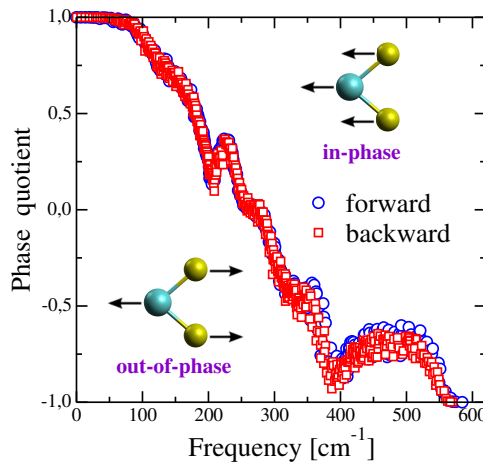


Figure 7 Frequency dependence of the phase quotient for the T-shaped MoS₂ nanoribbon with $W_{LR} = 3.0$ after a NEMD simulation in the forward (○-blue lines) and backward (□-red lines) directions ($T_0 = 300$ K and $\alpha = 0.1$).

References

- [1] J. Chen, G. Zhang, and B. Li, *J. Phys. Soc. Jap.*, 2010, **79**, 074604.
- [2] J. Shiomi and S. Maruyama, *Jap. J. Appl. Phys.*, 2008, **47**, 2005-2009.
- [3] R. N. Salaway and L. V. Zhigilei, *Int. J. Heat Mass Transfer*, 2014, **70**, 954-964.
- [4] A. Bodapati, P. K. Schelling, S. R. Phillpot and P. Keblinski, *Phys. Rev. B*, 2006, **74**, 245207.
- [5] P. K. Schelling and S. R. Phillpot, *J. Am. Chem. Soc.*, 2001, **84**, 2997-3007.